

# Supplementary material for 'Direct tunneling delay time measurement in an optical lattice'

A. Fortun, C. Cabrera-Gutiérrez, G. Condon, E. Michon, J. Billy and D. Guéry-Odelin  
*Laboratoire Collisions, Agrégats, Réactivité, IRSAMC, Université de Toulouse, CNRS, UPS, France*  
(Dated: June 21, 2016)

In this supplementary material, we provide an analysis of the out-of-equilibrium initial conditions investigated in the experiments in terms of Bloch bands and states. We then show results of numerical simulation to discuss: (i) the interference pattern for one and two wells, (ii) the onset of the quasi-isochronism as a function of the number of populated wells, and (iii) the fraction of atoms that tunnels through the barriers. A quantitative comparison of the Kapitza-Dirac diffraction method for the lattice depth calibration with the method based on the period measurement after a phase shift is detailed. A section is devoted to the results of other experiments and numerical simulations using the same offset technique in an optical lattice but for various other lattice depths. The last section is devoted to a simple semiclassical analysis of the traversal time for a single barrier.

## BAND ANALYSIS

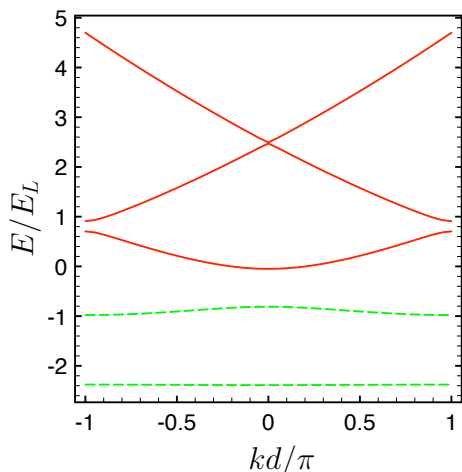


FIG. 1: (Color online). Band diagram for an attractive potential lattice of depth  $s_0 E_L$  with  $s_0 = 3.21$ . Bound level (green dashed line) and unbound level (red solid line)

The data presented in the main article have been carried out in an optical lattice of depth  $s_0 E_L$  with  $s_0 = 3.21$ . The corresponding band diagram is plotted in Fig. 1: only the two lower bands are entirely bounded, the bottom of the third band is slightly negative. The timescales associated to the energy diagram are:  $\hbar/(E_2(k=0) - E_1(k=0)) = 78.7 \mu\text{s}$  and  $\hbar/(E_3(k=0) - E_2(k=0)) = 163 \mu\text{s}$ .

As already explained, the initial state is prepared by a sudden shift of the optical lattice:  $\theta(0^+) = \theta_0$ . It is instructive to

work out the population  $\pi_n(\theta_0)$  of this initial state projected on the Bloch states  $|n, \mathbf{q} = \mathbf{0}\rangle$  for different initial conditions i.e. different initial angles  $\theta_0$ . They are summarized as histograms for  $n = 1, \dots, 6$  for the various initial angles that have been used in the experiment. For the two lowest angles,  $\theta_0 = 20^\circ$  and  $\theta_0 = 30^\circ$ , the population in the bound Bloch states (represented in green) is respectively 98.3 % and 93 %. The dynamics is therefore completely dominated by the two lowest bound states. Increasing the angle, the proportion of the initial wave function projected on the unbound Bloch states increases; it reaches 35 % for  $\theta_0 = 50^\circ$ .

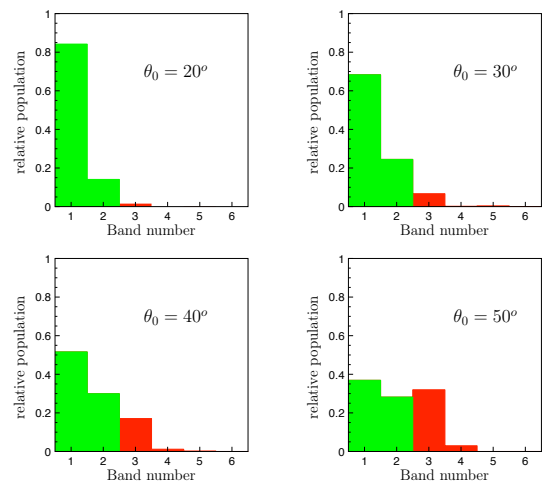


FIG. 2: (Color online). Probability of the initial state to be in the Bloch states  $|n, \mathbf{q} = \mathbf{0}\rangle$  for the six first bands  $n = 1, \dots, 6$ .

## NUMERICAL SIMULATIONS

In Fig. 3, we represent the dynamics of the wave packet inside one well and two wells after an initial offset  $\theta_0 = 20^\circ$ . As in the experiment, the simulation incorporates a time-of-flight, so that the pictures reflect the momentum space. The non harmonic character of a single well is apparent in the density plot for which the amount of stripes increases with time. It is worth noticing that with only two wells we recover a density plot qualitatively close to the experiment performed with a lattice: we indeed observe the tunneling packet and its delay with respect to the reflected packet, and the MZI effect.

In Fig. 4, we represent the density line  $p = 0$  as a function of the normalized time for different trapping conditions (this line corresponds to the central line - see for instance

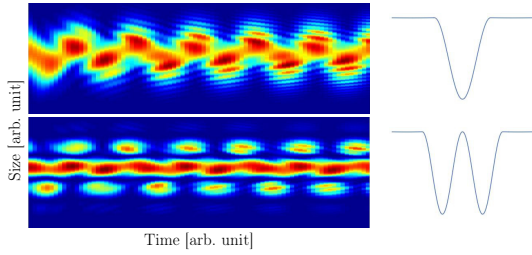


FIG. 3: (Color online). Time evolution of the ground state wave packet after an offset ( $\theta_0 = 20^\circ$ ), observed after time-of-flight, for a single well (upper part) and two wells (lower part) of depth  $s_0 E_L$  with  $s_0 = 3.21$ .

the dashed line in Fig. 4a - of figures obtained after a time-of-flight as in Fig. 3). For the smallest initial offset angle  $\theta_0 = 20^\circ$ , Fig. 4b reveals the emergence of a single oscillation frequency as the number of wells increases (see solid lines). We have also provided on the same graph the oscillation observed for a lattice (as in the experiment). With only 4 wells, we observe a periodicity that is already quite close to that of the lattice case. The dotted line corresponds to the oscillation observed for a harmonic trap whose angular frequency coincides with that obtained by the expansion of the potential wells about their minima. The period (normalized to  $\tilde{\omega}$ ) is smaller ( $\simeq 2.8$ ) for the harmonic case compared to that of the lattice ( $\simeq 4.3$ ). This difference is summarized systematically in Fig. 2 of the main article. These numerical results confirm that the oscillation is robust against the exact shape of the envelope. Additionally, in Figs. 4c,d,e we compare the oscillation frequency for  $\theta_0 = 20^\circ$  (dashed line) and  $\theta_0 = 70^\circ$  (solid line) for 2, 4 and 8 wells. We clearly see the “locking” to the same oscillation frequency when the number of wells increases. A similar curve for the lattice situation is finally provided in Fig. 4f. It reveals a small shift of the oscillations after five periods. This is the reason why we refer to this effect as a quasi-synchronization. In practice, the experiments presented in the main article investigate the time interval  $0 \leq \tilde{\omega}t \leq 5$ .

In figure 5a, we present the results of the numerical simulation of the Gross-Pitaevskii equation in the conditions of the experiment (to be compared with Fig. 3 of the main article). The simulation incorporates both the time evolution inside the lattice and the free evolution. We recover the same features as in the experiments: a delay between the packets  $D_1$  and  $D_2$  and a constructive interference (packet  $F$  of Fig. 1 of the main article). We have also extracted from the numerical simulation the evolution of the population  $\Pi_n$  in the momentum states  $nh/d$  with  $n = -1, 0, 1$  at the times for which we observe the maximum number of atoms in the packets  $D_1$  and  $D_2$ , and this for the 4 different initial angles  $\theta_0 = 20, 30, 40, 50^\circ$ . We clearly see in these graphs that  $\Pi_1(D_1) \simeq \Pi_{-1}(D_2)$  for all initial angles revealing that the splitting of the packet on the tunnel barrier is close to 50% transmission and 50% reflection. We also observe that the population  $\Pi_0$  in the momentum  $p = 0$  never vanishes for  $\theta_0 = 20^\circ$ . This is to be contrasted

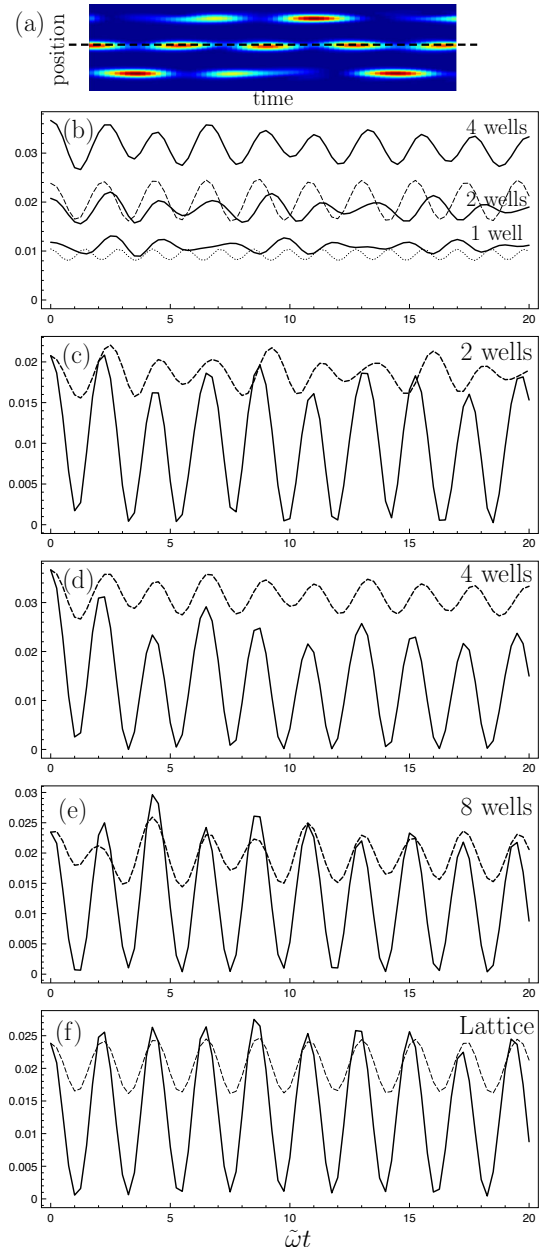


FIG. 4: (Color online) Numerical study of the quasi-synchronization. The density line  $p = 0$  obtained after a time-of-flight (black dashed line in a) is represented as a function of time (central line of plots similar to those of fig. 3) for various conditions. (b) initial shift angle  $\theta_0 = 20^\circ$  for 1,2,4 wells (solid lines), lattice (dashed line), harmonic trap associated to the bottom of the lattice sites (dotted line). (c), (d), (e) and (f) comparison of the central density line for  $\theta_0 = 20^\circ$  (dashed line) and  $\theta_0 = 70^\circ$  (solid line) for 2, 4, 8 wells and for the lattice.

with the data for  $\theta_0 = 40^\circ$  and  $\theta_0 = 50^\circ$  (see also Fig. 4 for  $\theta_0 = 70^\circ$ ). This can be simply interpreted by the fact that for the lowest angle the lowest Bloch band state remains mainly populated. It also means that there is a destructive interference for the population in  $p = 0$  when more bands (including unbound bands) are contributing to the interference signal.

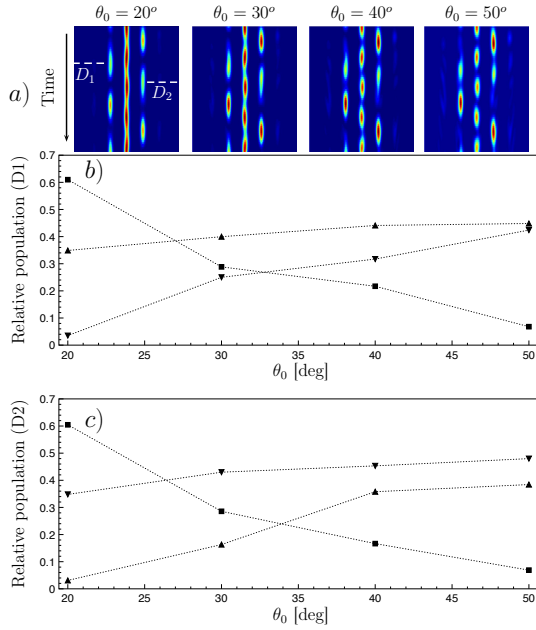


FIG. 5: (Color online). (a) Density plot obtained from the numerical simulation in the conditions of the experiment. Population in the different momentum classes  $\Pi_{-1} = -h/d$  ( $\blacktriangledown$ ),  $\Pi_0 = 0$  ( $\blacksquare$ ) and  $\Pi_1 = h/d$  ( $\blacktriangle$ ) at the times that correspond to the maximum of the density of the  $D_1$  (b) and  $D_2$  (c) packets (see white dashed lines on (a)).

### LATTICE DEPTH CALIBRATION

A standard method to calibrate *in situ* the depth of an optical lattice with a Bose Einstein condensate consists in using Kapitza-Dirac diffraction. For this purpose, one shines the optical lattice of depth  $V_0$  for a short amount of time  $\tau$  and observes the subsequent free evolution of the BEC. The spatial period  $d$  of the lattice generates a diffraction pattern of step  $ht_{\text{TOF}}/d$  when the expansion lasts for a sufficiently long time  $t_{\text{TOF}}$  to be dominated by the velocity field and no longer by the initial size. For short and intense pulses, the population in the different diffraction orders is well accounted by the so-called Raman-Nath regime for which the atomic motion is neglected during the light-matter interaction. In this limit, the zeroth order vanishes for a given pulse duration. This zero enables one to infer the lattice depth directly. In practice,  $\tau$  is varied from 1 to a few tens of  $\mu\text{s}$  and  $t_{\text{TOF}}$  is on the order of 20 ms. Figure 6a provides an example of such a time sequence for a lattice depth  $s = 2.8$ .

At low depth ( $s < 5.5$ ), the zeroth diffraction order does not vanish anymore. To get a reliable calibration, one should explore the diffraction pattern on longer time where the Raman-Nath approximation breaks down. In practice, we fit the population of each diffraction order with the appropriate Mathieu function[2–4] (see Fig. 6b).

In Fig. 6c, we summarize a set of experimental data for which we compare the lattice depth obtained from the Kapitza-Dirac diffraction method (black squares) with the one

deduced from the measurement of the period combined with numerical simulations as explained in the main text. We obtain a very good agreement between the two methods. Our method provides a calibration curve well fitted by

$$\tilde{\omega}T(s) = (a + bs + cs^2)e^{ds} \quad (1)$$

with  $\tilde{\omega} = 16\hbar/(md^2) = 24.3 \mu\text{s}$ ,  $a = 11.975$ ,  $b = -1.54017$ ,  $c = 0.2583$  and  $d = -0.2502$ . Using this relation it is therefore possible to infer the depth  $s$  from the experimental measurement of the period  $T$ .

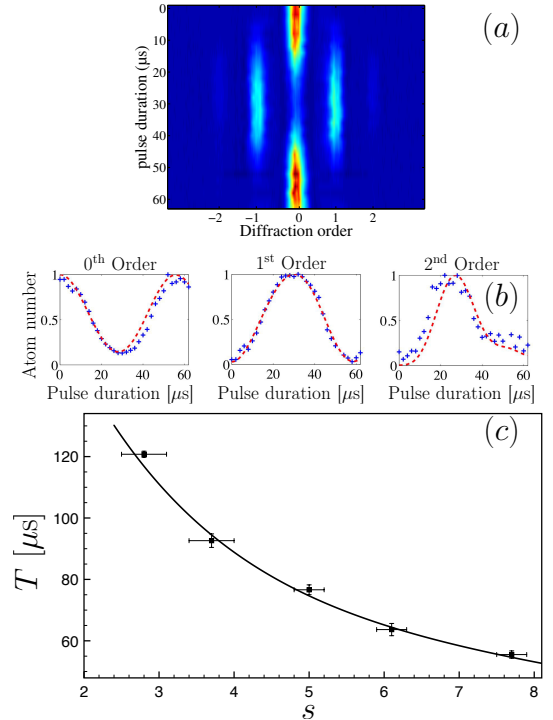


FIG. 6: (a) Evolution of the Kapitza-Dirac diffraction pattern with the pulse duration. Each horizontal line of the image corresponds to a time sequence in which the BEC is exposed to the lattice during the pulse duration and the picture is taken after a 20 ms time-of-flight. (b) Example of fit analysis of the diffraction order for  $s = 2.8$ , we clearly see that the zeroth order does not vanish as a function of the pulse duration. (c) Comparison between the Kapitza-Dirac diffraction method (black square) and the period measurement (see text) to determine the optical lattice depth without any adjustable parameter.

### THE DIFFERENT PARAMETER RANGES

The parameter space on which the tunnel delay is observed depends on both the lattice depth and the initial angle. In this section, we propose extra experimental (Fig. 7) and numerical data (Fig. 8) to detail the different situations encountered when the depth of the optical lattice is increased. We have indicated the threshold depths  $s_n$  below which  $n$  bands are entirely bound:  $s_1 = 0.8875$ ,  $s_2 = 3.0375$ ,  $s_3 = 6.425$  and

$s_4 = 11.05$ . Two experimental sequences have been taken in the region  $s < s_2$  (see Fig. 7). In this case, the contribution of the unbound states becomes important and the overlap between the unbound and tunnel packets renders more difficult an accurate determination of the tunnel time. The two contributions can be clearly identified in Fig. 7b: the packet due to unbound states is seen before the one originating from the tunneling. The experiment of the main text and two extra experimental data are proposed in the range of parameters  $s_2 < s < s_3$ . The data for  $s = 4.6$  clearly reveals the existence of tunneling, observed about the second turning point. This feature can also be clearly observed in the numerical data ( $s = 4.46$ ) in Fig. 8. The experiment carried out at a much larger depth,  $s = 15$ , exhibits a similar feature with a tunnel effect that is visible at the fourth turning point (see Fig. 7e). The dynamics of tunneling is therefore quite rich and observed on a large range of depths and initial angles. The choice  $s = 3.21$  of the main text corresponds to the simplest situation for which the tunneling is clearly observed and happens at the first turning point.

### SEMICLASSICAL EXPRESSION FOR THE TRAVERSAL TIME

The semiclassical traversal time  $\tau_t$  is given by [1]

$$\begin{aligned}\tau_t &= \frac{\partial}{\partial E} \left[ - \int_a^b \sqrt{2m(V(x) - E)} dx \right] \\ &= \int_a^b \left( \frac{m}{2} \right)^{1/2} \frac{dx}{\sqrt{V(x) - E}}\end{aligned}\quad (2)$$

where we have taken into account the boundary conditions  $V(a) = V(b) = E$ . If we apply this formula to a single barrier of the periodic potential, we get

$$\tau_t(\theta_0) = T_c(0) \frac{1}{2\pi} \int_{-u_a}^{u_a} \frac{du}{\sqrt{\cos^2 u - a}} \quad (3)$$

with  $T_c(0) = (2md^2/\hbar)s^{-1/2} = 69 \mu\text{s}$  the classical oscillation period about the minimum and  $u_a = \cos^{-1}(\sqrt{1 - \cos^2(\theta_0)})$ . In Table I, we summarize the traversal time values obtained for the different initial energies associated to different initial angle offsets  $\theta_0$ .

$\theta_0$ [deg]	20	30	40	50	60	70	80
$\tau_t(\theta_0)$ [ $\mu\text{s}$ ]	54	47	42	39	37	35.6	34.7

TABLE I: Traversal time for the different initial angles  $\theta_0$ .

We observe that this simple semiclassical analysis is not in agreement with our experiments and numerics. For the smallest angle, we observe a time twice smaller in the experiment. Furthermore, we obtain a much faster decrease of the tunneling time with the initial angle in the experiment than with this semiclassical calculation. This is certainly due to the increasing contribution of the unbound states. Remarkably we notice

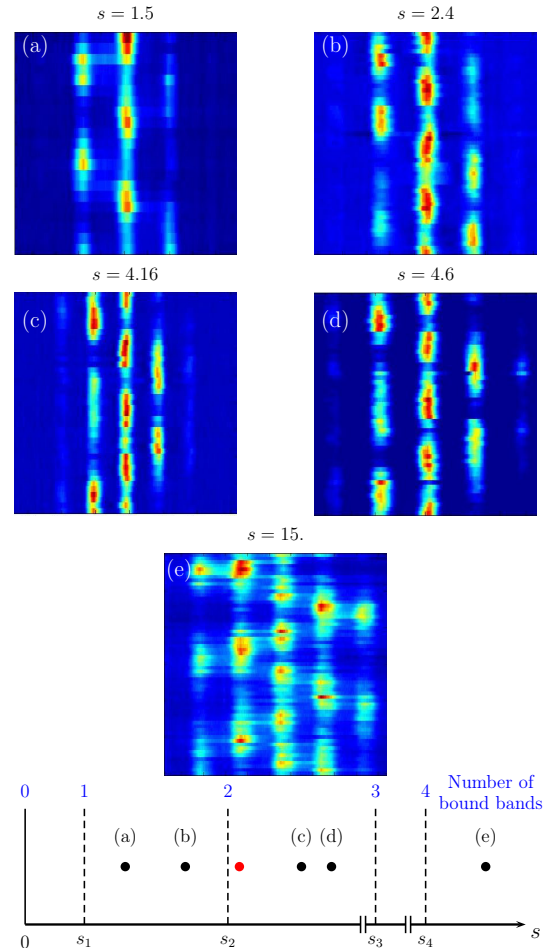


FIG. 7: Experimental results. Top: Experimental time sequence similar to that of Figure 1 of the main text but for different depths:  $s = 1.5$ (a),  $s = 2.4$ (b),  $s = 4.16$ (c),  $s = 4.6$ (d) and  $s = 15$ (e) and with an initial shift angle  $\theta_0 = 30^\circ$ . Bottom: Sketch of the different regimes depending on the lattice depth  $s$ .  $s_n$  is the value for which when  $s < s_n$ , the lattice has  $n$  bound bands ( $s_1 = 0.8875$ ,  $s_2 = 3.0375$ ,  $s_3 = 6.425$  and  $s_4 = 11.05$ ).

that with just one lattice depth and by varying the initial angle, we can rule out this naive model.

The discrepancy between the experimental results and this naive semiclassical approach presented here originates from the fact that the tunnel effect that we studied experimentally occurs in a space dressed by the optical lattice. As already emphasized, the simple center of mass oscillation is strongly renormalized by the periodic potential. The models that have been developed so far in the literature to determine the tunnel traversal time have been worked out in free space. Our experimental results should trigger a theoretical effort to extend the different approaches to dressed environment for a proper comparison.

[1] M. Büttiker and R. Landauer, Phys. Rev. Lett. **49**, 1739 (1982).

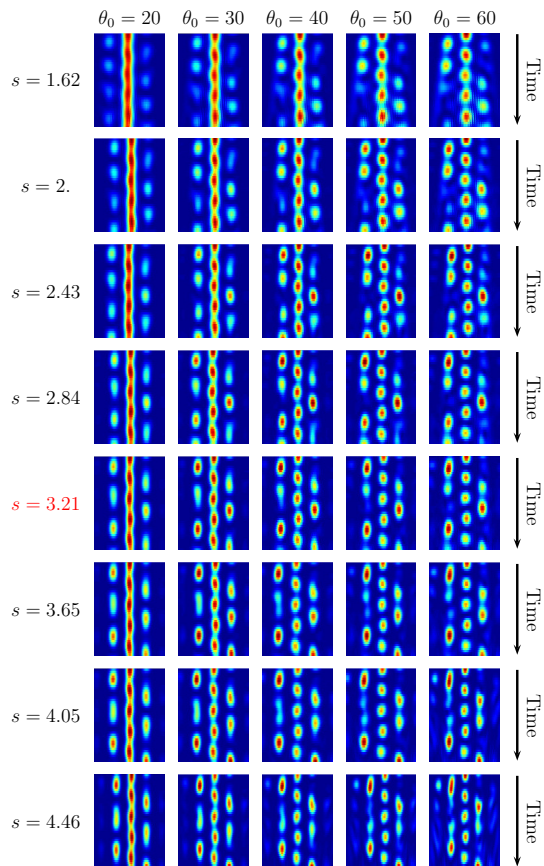


FIG. 8: Numerical results. Evolution of the diffraction pattern for different depth ( $s$  parameter) and different initial angle offset  $\theta_0$ . The parameters chosen in the main text correspond to  $s = 3.21$ .

- [2] M. Horne, I. Jex, and A. Zeilinger, Phys. Rev. A **59**, 2190 (1999).
- [3] J. H. Huckans, I. B. Spielman, B. Laburthe Tolra, W. D. Phillips, and J. V. Porto, Phys. Rev. A **80**, 043609 (2009).
- [4] B. Gadway, D. Pertot, R. Reimann, M. G. Cohen, and D. Schneble, Optics Express **17**, 19173 (2009).